International Journal of Thermal Sciences 203 (2024) 109167

Contents lists available at ScienceDirect

International Journal of Thermal Sciences

journal homepage: www.elsevier.com/locate/ijts

The local heat transfer characteristics associated with mixed convective developing flow through a horizontal tube exposed to a uniform wall temperature boundary condition

Mark J. Coetzee [a], Deniel Steyn [a], Marilize Everts [a,b,*]

[a] Department of Mechanical and Aeronautical Engineering, University of Pretoria, Pretoria, 0028, South Africa
[b] Department of Mechanical Engineering, University College London, London, WC1E 7JE, United Kingdom

ARTICLE INFO

Keywords:
Developing flow
Heat transfer
Laminar flow
Mixed convection
Uniform wall temperature

ABSTRACT

Extensive research has been conducted on the heat transfer characteristics related to the boundary conditions present in phase-change applications. However, there remains a fundamental gap in understanding the local heat transfer characteristics of mixed convective laminar flow exposed to a uniform wall temperature boundary condition. Furthermore, there is a disparity between numerical and experimental studies investigating this boundary condition. This study addresses these gaps by being the first to experimentally investigate the local heat transfer characteristics of developing laminar flow through a horizontal tube exposed to a uniform wall temperature boundary condition. A novel experimental setup was developed to measure the mean fluid temperatures along a 5 m-long copper tube with an inner diameter of 4.9 mm. While the local results indicated an increase in wall temperature along the test section, the average Nusselt numbers correlated well with literature, indicating that similar temperature trends existed in prior experimental studies. The local heat transfer characteristics for developing laminar uniform wall temperature flow were divided into four regions: (1) Free Convection Developing, (2) Free Convection Governing, (3) Sustained Free Convection, and (4) Diminishing Heat Transfer. Free convection effects were found to increase near the inlet of the tube and the associated secondary flow assisted the flow in becoming fully developed. However, due to the decreasing wall-fluid temperature differences, free convection effects could not be sustained, and heat transfer eventually diminished as the fluid temperatures approached the wall temperatures.

Nomenclature

A	Area	m^2
Cp	Specific heat capacity	J/kg.K
D	Diameter	m
g	Gravitational acceleration	m^2/s
Gr	Grashof number	
Gz	Graetz number	
h	Heat transfer coefficient	$W/m^2.°C$
k	Thermal conductivity	W/m.K
L	Length	m
$\dot{m}$	Mass flow rate	kg/s
Nu	Nusselt number	
p	Perimeter	m
Pr	Prandtl number	
R	Thermal resistance	°C/W
Re	Reynolds number	

(*continued on next column*)

(*continued*)

T	Temperature	°C
x	Distance from inlet	m
Greek letters		
β	Thermal expansion coefficient	1/K
μ	Dynamic viscosity	kg/m.s
ν	Kinematic viscosity	m^2/s
Subscripts		
avg	Average	
b	Bulk/bottom	
bath	Bath temperature	
e	End of test section	
f	Fluid	
G	Gnielinski	
i	Inlet of test section/internal	
L	Average over test section	
lm	Logarithmic mean temperature difference	

(*continued on next page*)

* Corresponding author. Department of Mechanical Engineering, University College London, London, WC1E 7JE, United Kingdom.
E-mail address: m.everts@ucl.ac.uk (M. Everts).

https://doi.org/10.1016/j.ijthermalsci.2024.109167
Received 6 February 2024; Received in revised form 24 April 2024; Accepted 17 May 2024
Available online 24 May 2024
1290-0729/© 2024 The Authors. Published by Elsevier Masson SAS. This is an open access article under the CC BY license (http://creativecommons.org/licenses/by/4.0/).

(*continued*)

m	Mean
n	Measuring station
N	Number of bath sections
o	End of bath section/outside
t	Top
w	Wall
wb	Water bath section
x	Local
Abbreviations	
DHT	Diminishing Heat Transfer
FC	Forced convection
FCD	Free Convection Developing
FCG	Free Convection Governing
FD	Fully developed
MC	Mixed convection
SFC	Sustained Free Convection
UHF	Uniform heat flux
UWT	Uniform wall temperature

1. Introduction

The global community is attempting to reduce the dependency on fossil fuel resources. Insight of these initiatives and legislation are being implemented to encourage corporations to invest in energy-efficient systems. An example of such a system is the development of heat recovery chillers for large-scale building air-conditioning systems. These chillers use phase-change heat exchangers to recover wasted heat from the condensing cycle of the refrigerant direct expansion system employed by air-cooled chillers. The recovered heat is then repurposed to heat water for domestic use in establishments such as hotels, hospitals, and offices. Phase-change heat exchangers use the latent heat of evaporation to transfer thermal energy between two fluids [1]. In heat recovery chillers, the two-phase condensing refrigerant is used to heat the flow of water. This process maintains the tube walls of the heat exchanger at a constant temperature due to the phase-change of the refrigerant [2]. This is commonly classified as a uniform wall temperature (UWT) boundary condition in heat transfer analyses.

There is a continuous need to improve the efficiency of such heat exchangers while decreasing the size to minimise space and material requirements. Therefore, manufacturers make use of compact heat exchangers for heat recovery chillers [3]. As the size of the flow-channels or tubes are decreased, the flow rates are also decreased, and heat exchangers start operating in the laminar flow regime. This flow regime is known for its low pressure drops and thus low operational running costs. However, the heat transfer coefficients are lower than for turbulent flow. Besides enhancing heat transfer using nanofluids [4–7], recent studies [8–10] proved that mixed convective flow effectively enhances heat transfer with a minimal increase in pressure drop. Furthermore, as the heat transfer coefficients of developing flow are higher than for fully developed flow, flow disturbances are often incorporated in heat exchangers to disturb the development of the thermal and hydrodynamic boundary layers [11]. Therefore, the laminar flow regime offers an ideal environment for studying mixed convective developing flow. Improving our fundamental understanding of developing mixed convective laminar flow for UWT boundary condition applications will enable design engineers to improve the efficiency of compact heat exchangers operating in the laminar flow regime.

However, as will be shown in this study, there is a deficit in the understanding of the heat transfer that occurs in such applications, especially when considering mixed convective developing flow. The deficit has come about because of the limited number of studies that investigated UWT flow, compared to (uniform heat flux) UHF flow. Furthermore, to date no experimental study has specifically focussed on the local heat transfer characteristics through a horizontal tube exposed to a UWT boundary condition.

The extent of the lack of insight into mixed convection flow exposed to a UWT boundary condition flow is visualised in Fig. 1, where the

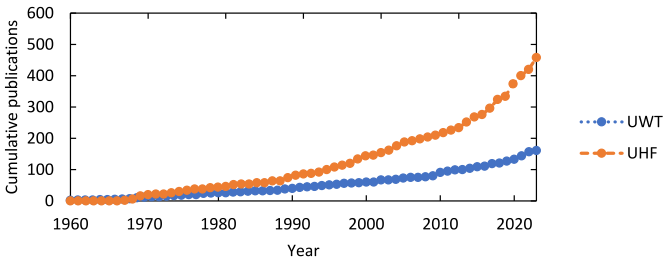

Fig. 1. Cumulative number of publications containing the phrase "Uniform heat flux" or "Uniform wall temperature" for "Horizontal tubes" in the title, abstract or keywords per year according to Scopus since 1960 (Accessed: April 2024).

accumulative publications (cited in Scopus since 1960) on UWT and UHF flow through horizontal tubes are compared. UHF flow was extensively investigated experimentally, and special attention was given to mixed convective and developing flow by authors such as Ghajar and Tam [12], Everts and Meyer [9], and Meyer [13], while Fig. 1 indicates that UWT flow has not received comparable attention over the past three decades. The number of UHF and UWT publications was approximately equal in 1981 and by 2017, the number of UHF publications were 50 % greater compared to 1981. The reason for this is probably that UHF offers greater heat transfer rates in the laminar flow regime [2,14] and is easier to investigate experimentally.

Most applications contain mixed convective flow due to the temperature differences and thus density differences that exist inside the tubes. The advances in mixed convective flow have been largely attributed to experimental studies [15–20] and recent numerical studies [10,21] of UHF flow. Together with rigorous experimental studies, numerical studies are valuable in providing a deeper understanding of the flow and heat transfer phenomena that give rise to the heat transfer trends. Everts and Meyer [22] reported that for UHF flow, it is challenging to experimentally investigate forced convective flow, while this is easier to investigate numerically, as shown by turbulent numerical studies such as Taler [23]. Due to the lack of studies focusing on UWT flow in comparison to UHF flow, there are only a handful of studies that can be compared. Table 1 summarises the published experimental studies on mixed convective UWT flow for horizontal smooth tubes in chronological order. The most recent theoretical work was done in the 1980s and 1990s by Hieber [24], Coutier and Greif [25] and Shome and Jensen [26]. The gap between one of the most recent experimental publications for flow in a smooth straight tube (Bertsche et al. [20]) and the preceding publication (Coutier and Grief [25]) is nearly 30 years.

Jackson et al. [15] used a steam jacket to achieve a UWT boundary condition, and experiments were conducted using air in the laminar, transitional, and turbulent flow regimes. They highlighted the impact that the Graetz number, Grashof number, and the length-to-diameter ratio had on predicting heat transfer rates for UWT flow. Oliver [16] proposed that once the length-to-diameter ratio exceeded 70, the ratio had a negligible effect on predicting the influence of free convective effects. Depew and August [18] noted that due to the decreasing wall-fluid temperature difference along the tube length, the influence of free convective effects diminishes along a test section. Therefore, free convection effects are expected to be more prominent in shorter tubes, due to the steeper wall-fluid temperature gradient, but insufficient experimental data was available to verify this.

Yousef and Tarasuk [19] proposed that UWT flow could be divided into three regions: (1) at the inlet where free convection effects are dominant, (2) further down the tube where free convection effects diminish and forced convection effects become dominant, and (3) near the end of the tube where the Nusselt number would become constant. However, it was found that the average Nusselt number at the end of the tube was lower than the fully developed forced convection Nusselt number of 3.66. Bertsche et al. [27] further emphasized the lack of

Table 1
Summary of the available experimental data from literature for mixed convective flow in smooth horizontal tubes with a UWT boundary condition.

Author	Year	Fluid	Reynolds number	Prandtl number	Data points	Diameter [mm]	Length [m]	Local or average measurements	Entrance problem
Jackson et al. [15]	1961	Air	1 300–2 300	0.71	98	98.4	3.048	Average	Combined
Oliver [16]	1962	Water	141–1 580	4.32–9.45	23	12.7	0.9144	Average	Single
		Ethyl alcohol		4.8–7.0	20				
		Glycerol-water		62–326	24				
Brown & Thomas [17]	1965	Water	235–1 240	3.5–7.4	105	12.7 25.4	0.9144–1.402 0.9144	Average	Combined
Depew & August [18]	1971	Water	91–1 321	5.7–8.0	16	19.05	0.5664	Average	Single
		Ethyl alcohol	68–1 453	14.2–16.1	13				
		Glycerol-water	73–1 382	328–391	11				
Yousef & Tarasuk [19]	1982	Air	138–1 179	0.7	228	25	0.05–1.2	Average	Combined
Bertsche et al. [27]	2016	Glycerol-water	400–2 300	7.0–16.0	15	2.6	0.22	Average	Combined

experimental data available for UWT flow and noted that there is little to no data available for Reynolds numbers between 1 000 and 4 000, especially for high Prandtl numbers, i.e., $10 < Pr < 90$.

A key challenge in achieving a true UWT boundary condition lies in maintaining a uniform wall temperature along the entire test section and Table 1 shows that this might not have received detailed attention in previous studies. Bertsche et al. [5] employed a parallel flow heat exchanger design to attain a UWT boundary condition. However, insufficient evidence was provided to justify their claim of achieving a uniform wall temperature along the test section. Despite having 36 thermocouples along their test section and a reported temperature accuracy of ±0.05 °C, a plot of their temperature distribution was not provided. Brown and Thomas [18] did not measure the wall temperatures and relied on an average of the inlet and outlet temperatures from their water jacket, while Oliver [17] used a single thermocouple to measure the wall temperature. Yousef and Tarasuk [20] used a heating wire technique, typically used by UHF studies, to obtain a UWT boundary condition. Furthermore, their multi-sectioned design could not reliably repeat the boundary condition to enable analysing local heat transfer characteristics. Therefore, to date, no experimental study has investigated the wall temperature uniformities along their test sections or implemented methods to measure the local mean fluid temperature distribution along a test section. This limited investigations to analysing average heat transfer rates.

The limited test section lengths used by the reported studies raise the question of whether fully developed flow has been achieved and investigated. Brown and Thomas [18] experimented with the longest test section with a length-to-diameter ratio of 110, whereas recent UHF experiments by Everts and Meyer [22,28] used a length-to-diameter ratio up to 1 300. Using the most recent correlations developed by Everts and Meyer [22] to calculate the thermal entrance length for the test section of Brown and Thomas [17], reveals that they would have required a test section with a length-to-diameter ratio of 390. The expected thermal entrance lengths for the other studies in Table 1 were also calculated and predicted that none had sufficient lengths to ensure fully developed flow. Although the correlations developed by Everts and Meyer [22] are intended for UHF flow, they were considered the most accurate available to estimate the thermal entrance lengths for UWT flow. The limitation to short test sections emphasises the difficulty of achieving a uniform temperature distribution along a test section as well as the lack of fully developed mixed convective UWT boundary condition studies.

The published heat transfer correlations for mixed convective UWT flow are summarised in Table 2. Despite the shortcomings of the studies that developed these correlations, they are some of the only available to design engineers and it is important to investigate their accuracy and suitability for future designs.

Table 2
Average laminar Nusselt number correlations for mixed convective UWT flow.

Jackson et al. [15] (1961) (1)

$$Nu_L = 2.67\left[Gz_b^2 + (0.0087)^2 (Gr_{lm}\, Pr)_w^{1.5}\right]^{\frac{1}{6}}$$
$$1\,300 \le Re \le 2\,300\ ;\ Pr \ge 0.7$$
$$1.57 \times 10^6 \le Gr \le 3.14{\times}10^6$$

Oliver [16] (1962) (2)

$$Nu_L \left(\frac{\mu_w}{\mu_b}\right)^{0.14} = 1.75\left[Gz_{lm} + 5.6\times 10^{-4}\left(Gr_m\, Pr_m \frac{L}{D}\right)^{0.7}\right]^{1/3}$$
$$140 \le Re \le 1\,600\ ;\ 4.8 \le Pr \le 7$$
$$4.9 \times 10^4 \le Gr \le 1.6{\times}10^5$$

Brown and Thomas [17] (1965) (3)

$$Nu_L \left(\frac{\mu_w}{\mu_b}\right)^{0.14} = 1.75\left[Gz + 0.012\left(GzGr^{\frac{1}{3}}\right)^{\frac{4}{3}}\right]^{\frac{1}{3}}$$
$$230 \le Re \le 1\,240\ ;\ 3.5 \le Pr \le 7.4$$
$$2.9 \times 10^4 \le Gr \le 4.9{\times}10^6$$

Depew and August [18] (1971) (4)

$$Nu_L \left(\frac{\mu_w}{\mu_b}\right)^{0.14} = 1.75\left[Gz + 0.12\left(GzGr^{\frac{1}{3}}\, Pr^{0.36}\right)^{0.88}\right]^{\frac{1}{8}}$$
$$70 \le Re \le 1\,450\ ;\ 5.7 \le Pr \le 8$$
$$0.7 \times 10^5 \le Gr \le 5.8{\times}10^5$$
Thermally developing

Yousef & Tarasuk [19] (1982) (5)

$$Nu_L \left(\frac{\mu_w}{\mu_b}\right)^{0.14} = 1.75\left[Gz + 0.245\left(Gz^{1.5}Gr^{\frac{1}{3}}\right)^{0.882}\right]^{\frac{1}{3}}$$
$$140 \le Re \le 1\,200\ ;\ Pr \ge 0.7$$

In contrast to the advances in mixed convection, the advances in forced convective flow have been mostly achieved by analytical and numerical work [29–34]. The available Nusselt number correlations are summarised in Table 3. This table also highlights the key differences between the progress that has been made for forced and mixed convective flow: (1) unlike mixed convection, forced convective developing flow has been extensively investigated by numerical and analytical studies, and (2) varying wall temperature uniformities of the boundary conditions. As noted in Table 1, possible non-uniformities in

Table 3
Laminar heat transfer correlations for developing forced convective UWT flow. The percentage deviation of the correlations was obtained from Bennet [38].

Churchill and Ozoe [29], (1973) (6)

$$\frac{Nu_x + 1.7}{5.357\left[1+\left(\frac{\pi Gz_x}{388}\right)^{\frac{8}{9}}\right]^{\frac{3}{8}}} = \left[1+\left(\frac{\pi Gz_x/284}{\left[1+(Pr/0.0468)^{\frac{2}{3}}\right]^{\frac{1}{2}}\left[1+\left(\frac{\pi Gz_x}{388}\right)^{\frac{8}{9}}\right]^{\frac{3}{4}}}\right)^{\frac{4}{3}}\right]^{\frac{3}{8}}$$

$$Re \leq 2\,300$$

Percentage deviation : -0.7% to $+8\%$

Shome and Jenson [30], (1993) (7)

$$Nu_x = Nu_x^{Grtz}\left[1+0.004\left(Gz_x^{-1}\,Pr\right)^{-1.0}\right]^{0.12}$$

$$Nu_x^{Grtz} = \begin{cases} \dfrac{1.022}{Gz_x^{-0.3366}} - 0.3856 & Gz_x^{-1} \leq 0.001 \\ 3.6568 + 0.2249/Gz_x^{-0.4956}\; exp\left(-55.9857 Gz_l^{-1}\right) & 0.001 < Gz_x^{-1} \end{cases}$$

$$Re < 2\,300, Pr > 0.7$$

Percentage deviation : -15% to $+3.3\%$

Muzychka and Yovanovich [31], (2004) (8)

$$Nu_x = \left[\left(\frac{0.564\Big/Gz_x^{-\frac{1}{2}}}{\left[1+\left(1.664\,Pr^{\frac{1}{6}}\right)^{\frac{9}{2}}\right]^{\frac{2}{9}}}\right)^m + \left(\left[0.409\left(\frac{64}{4Gz_L^{-1}}\right)^{\frac{1}{3}}\right]^5 + 3.657^5\right)^{\frac{m}{5}}\right]^{\frac{1}{m}}$$

(9)

$$Nu_L = \left[\left(\frac{1.128\Big/Gz_L^{-\frac{1}{2}}}{\left[1+\left(1.664\,Pr^{\frac{1}{6}}\right)^{\frac{9}{2}}\right]^{\frac{2}{9}}}\right)^m + \left(\left[06135\left(\frac{64}{4Gz_L^{-1}}\right)^{\frac{1}{3}}\right]^5 + 3.657^5\right)^{\frac{m}{5}}\right]^{\frac{1}{m}}$$

$$m = 2.27 + 1.65\,Pr^{\frac{1}{3}}$$

$$Re < 2\,300, Pr > 0.1$$

Percentage deviation : -14% to $+4.6\%$ and -15% to $+1.2\%$

Gnielinski [32], (1975) (10)

$$Nu_x = \left(\left(\frac{Gz_x^3/32}{1+22\,Pr}\right)^{\frac{1}{2}} + \left(1.077 Gz_x^{\frac{1}{3}} - 0.7\right)^3 + 0.7^3 + 3.66^3\right)^{\frac{1}{3}}$$

(11)

$$Nu_L = \left(\left(\frac{2Gz_L^3}{1+22\,Pr}\right)^{\frac{1}{2}} + \left(1.615 Gz_x^{\frac{1}{3}} - 0.7\right)^3 + 0.7^3 + 3.66^3\right)^{\frac{1}{3}}$$

$$Re \leq 2\,300$$

Percentage deviation : $+14\%$ and -0.6% to $+8.7\%$

Jacimovic et al. [34], (2018) (12)

$$Nu_L = 3.657 + \frac{0.06 Gz_L^{1.117}}{1+0.031\,Pr^{0.08} Gz_L^{0.779}}$$

Percentage deviation : -17% to $+8.9\%$

Bennet [33], (2019) (13)

$$Nu_L = \frac{\left(5.079 Gz_L^{1.13} + 146.9\right)^{0.295} - 0.701}{tanh\left[2.434\left(Pr\,Gz_L^{-1}\right)^{\frac{1}{6}}\left(1+\left(0.4022\,Pr\,Gz_L^{-1}\right)^{0.2894}\right)^{0.5758}\right]}$$

(14)

$$Nu_x \Big/ Nu_L = 1 - \frac{\left(Gr_x^{1.13}/3\right)\left(Gr_x^{1.13}+28.92\right)}{1-\frac{0.4338}{\left(Gr_x^{1.13}+28.92\right)^{0.295}}} - \frac{2-\left(1+\left(0.4022\,Pr\,Gr_x^{-1}\right)^{0.2894}\right)^{-1}}{3\,sinh\left(2F_{Pipe}^T\right)\Big/F_{Pipe}^T}$$

$$F_{Pipe}^T = 2.434\left(Pr\,Gr_x^{-1}\right)^{1/6}\left(1+\left(0.4022\,PrGr_x^{-1}{}^{0.2894}\right)^{0.5758}\right.$$

$$Re < 2\,300, Pr > 0.7$$

Percentage deviation : -1.5% to $+2.3\%$

the wall temperature existed along the test sections, while theoretical applications consider the wall temperature to be perfectly uniform [33]. The available analytical and numerical studies have not yet investigated the effect of wall temperature non-uniformities on the flow. Therefore, none of these studies have fully replicated the actual conditions that experimental researchers face. Despite the discrepancy between the experimental and theoretical studies, the forced convection correlations listed in Table 3 have been shown to predict experimental results with reasonable accuracy [20,35–37]. This suggests that it might be worthwhile to investigate to what extent these correlations are applicable to mixed convective flow.

The final key difference between experimental and theoretical studies lies in the respective validation procedures. Studies like Yousef and Tarasuk [19], Brown and Thomas [17], and Oliver [16] did not make use of any analytical relationships when validating their results. In contrast, Bennett [33], Churchill [29], Jacimovic et al. [34], and Shome and Jensen [30] did not make use of any experimental relationships to validate their results. This lack of agreement between experimental and theoretical studies is most probably because of scant literature. Hieber [24] and Shome and Jensen [26] are among the few analytical and numerical studies that have investigated mixed convective flow. However, it is worth noting that the analysis of Shome and Jensen [26] omitted effects such as property variation and axial wall conduction, which exists in general heat transfer conditions [2].

While analytical and numerical studies focused on forced convective flow and experimental studies on mixed convective flow, the lack of agreement between experimental and theoretical studies has slowed down the understanding and application of developing mixed convective UWT flow. A thorough fundamental understanding of the heat transfer characteristics associated with developing UWT flow is required to enable engineers to improve the efficiency of compact heat exchangers operating in the laminar flow regime. Therefore, the purpose of this study was to experimentally investigate the temperature uniformity and local heat transfer characteristics of laminar flow through horizontal tubes exposed to a UWT boundary condition. Special attention was also given to the associated wall temperature uniformities, and a novel experimental approach was developed to measure the mean fluid temperatures along the tube length without obstructing the flow.

2. Experimental setup and test matrix

To experimentally investigate the local heat transfer characteristics of UWT flow, the mean fluid temperatures along the test section are required. Therefore, a novel approach was implemented to measure the mean fluid temperatures along the test section without obstructing the flow. The experimental setup depicted in Fig. 2 consisted of two flow loops, one to achieve a UWT along a test section (bath supply) and the other to supply flow to the test section (test section supply). A 5 m-long water bath was divided into five isolated 1 m-long sections. Experiments were first conducted using one section only (thus a test section length of 1 m), while the remainder of the test section was insulated, and the other four bath sections were empty. Thereafter, for the remaining 4 m, the test section was artificially lengthened by removing the insulation from the next 1 m-long section, filling the bath section with water, and

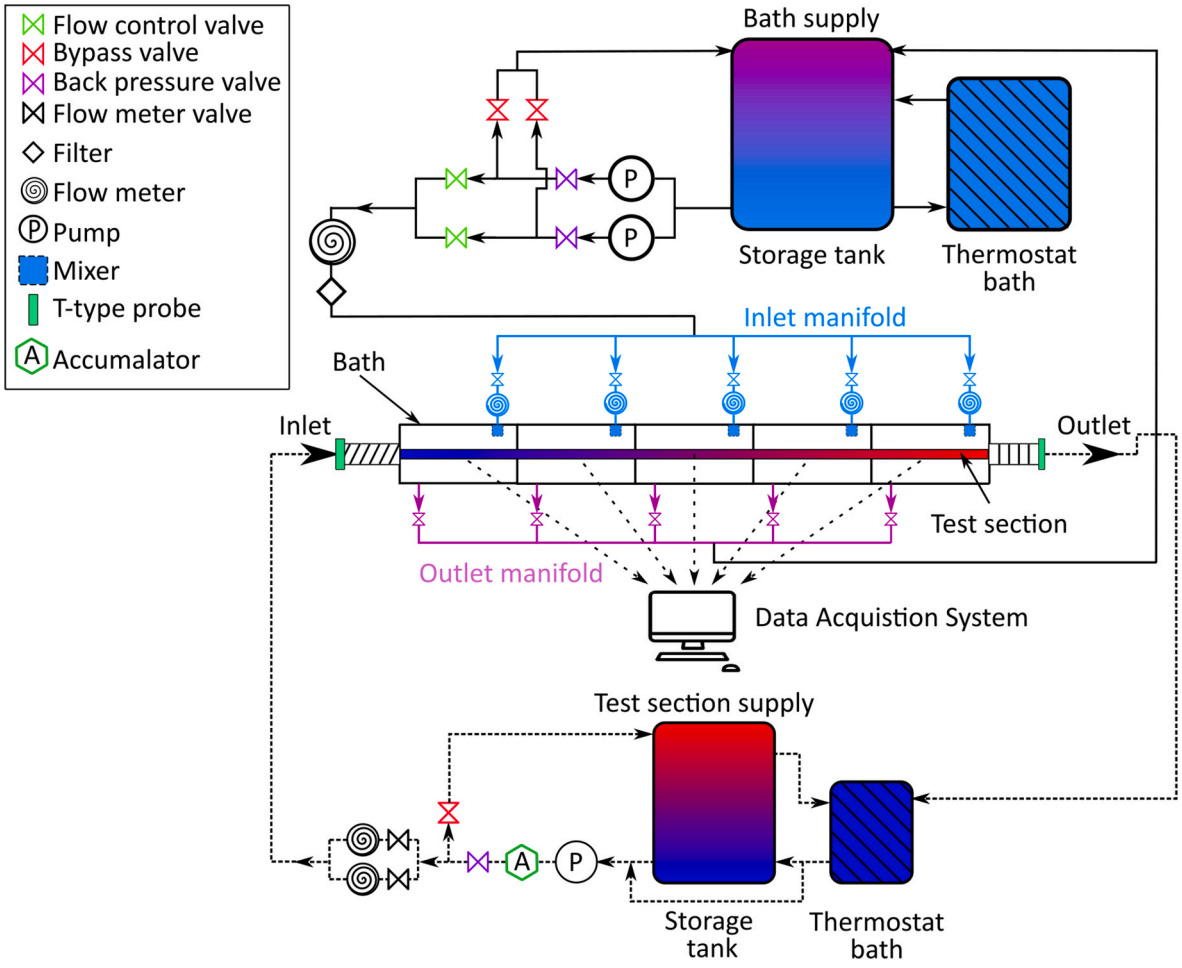

Fig. 2. Schematic of the overall experimental setup which consisted of one flow loop to apply a UWT boundary condition (solid lines) and another flow loop to supply water at a constant temperature to the test section (dotted lines).

repeating the experiments using two, three, four and lastly, five sections. The fluid temperature at the end of each section was measured at the outlet of the test section (after the fifth bath section) but translated to the end of the respective section as the heat losses along the insulated sections were considered negligible. Therefore, it was assumed that the fluid temperature measured at the outlet of the test section was the same as the fluid temperature at the end of the last uninsulated bath section. The mean fluid temperature along the test section was then predicted by performing a non-linear least squares curve fit through the five fluid temperature measurements recorded for each testing scenario and the measured inlet temperature.

Each bath section was supplied with water from the bath supply flow loop (solid lines in Fig. 2), which used a thermostat-controlled bath and a storage tank to control the temperature of the water supplied to each section. The bath sections were insulated using 40 mm-thick Armaflex insulation (thermal conductivity of 0.034 W/m.K) to minimise heat losses to the environment. Water was pumped to the inlet manifold using two pumps placed in parallel. The flow rate into each section was varied by adjusting the valves placed at the outlet manifold and the back pressure of the pump. The inlet manifold housed five flow meters to ensure identical flow rates to each section, and the optimal flow rate to the bath sections was investigated. Experiments were conducted using the first bath section, and the flow rate to the bath was varied between 1 and 7 ℓ/min. The bath temperature was set to 25 °C, and water flowed through the test section at a Reynolds number of 600. It was found that although higher flow rates improved the wall temperature uniformity, no significant improvement was found when increasing the flow rate beyond 5 ℓ/min.

Furthermore, care was taken to prevent insufficient mixing around the test section, as this could lead to wall temperature non-uniformities. A mixer was placed at the inlet of each section to agitate the flow and assist in achieving a uniform temperature distribution across the tube. The effect of the mixer on the wall temperature uniformity was investigated in the second bath section by comparing the results with and without the mixer. When no mixer was used, a local hot spot existed at the inlet of the section, where the flow impinged the tube. When using the mixer, the temperature difference between the inlet and outlet decreased and a localised temperature drop at the outlet of the previous section was also improved. Therefore, it was concluded that the mixer improved the wall temperature uniformity.

The test section loop (dotted lines in Fig. 2) ensured that the water supplied to the test section was kept at a constant temperature of 20 °C with the use of another thermostat-controlled bath and storage tank. The flow rate to the test section was controlled using frequency drives connected to the pump and was measured using two Coriolis mass flow meters of varying capacities. As this study focused on laminar flow only, the flow meter with a range of 0–180 ℓ/h was selected to conduct the experiments for Reynolds numbers between 600 and 2 400. A flow calming section was attached to the test section to obtain a square-edged inlet geometry and simultaneously thermally and hydrodynamically developing flow from the inlet of the test section. The flow calming section was insulated with 40 mm-thick Armaflex insulation to prevent heat transfer to or from the environment. The temperature at the inlet of the test section was measured with a T-type thermocouple probe placed at the inlet of the flow calming section. A mixing section was placed after the test section to mix the fluid before measuring the outlet temperature using another T-type thermocouple probe. Both thermocouple probes were calibrated in a thermostat-controlled bath between 15 °C and 40 °C to within an accuracy of 0.1 °C.

The test section in Fig. 3 was constructed from a 5 m-long hard drawn smooth copper tube with an inner diameter of 4.9 mm and an outer diameter of 6.5 mm. The wall temperature along the test section was measured using T-type thermocouples with a wire diameter of 0.25 mm. Twenty-six thermocouple stations, each containing three thermocouples spaced 90° around the periphery, were positioned along the test section. As indicated in Fig. 3, the placement of the third thermocouple alternated between left and right along the length of the test section. The thermocouples for bath stations A to F were spaced close to one another to capture the developing temperature profile in the first section. The thermocouples in the subsequent bath sections were equally spaced, with thermocouple stations placed at the inlet and outlet of each section to monitor any possible local hot spots. In addition, the fluid temperature in each bath section was measured with two free floating thermocouples placed at the inlet and outlet of each section, as indicated by the green markers in Fig. 3.

The thermocouples were fixed to the test section using the method described by Everts and Meyer [39]. A small indentation with a depth of approximately 0.4 mm was drilled into the test section and filled with solder. After preparing the junction at the tip of the thermocouple, a soldering iron was used to press the junction into the heated indentation. This ensured that the thermocouple was in direct contact with the wall of the test section and covered in solder. The thermocouples were calibrated in-situ over a range of 15 °C–40 °C to within an accuracy of 0.1 °C against the inlet and outlet T-type probes by pumping water from a thermostat bath through the test section.

Table 4 summaries the experiments conducted at different mass flow rates and bath temperatures. A total of 150 tests were conducted, which consisted of 150 flow rate measurements and 12 000 temperature measurements. During the analysis of the results, it was found that at a set bath temperature of 35 °C, the bath temperature increased along the

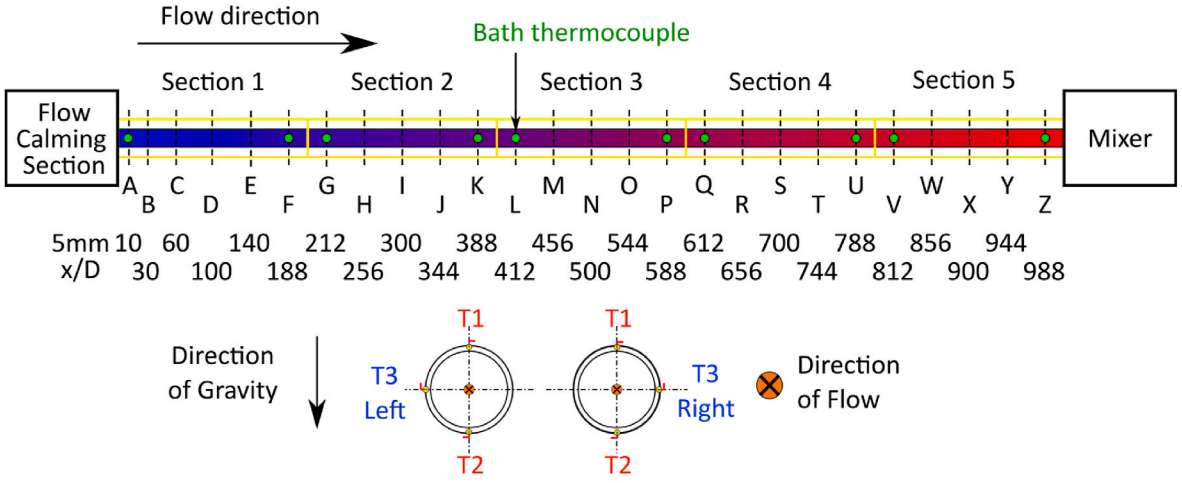

Fig. 3. Schematic of the axial positions of the thermocouple stations (dotted lines) along the test section and the bath thermocouples (green markers). The cross-sectional thermocouple station layout indicates the alternating thermocouple stations along the test section.

Table 4
Experimental test matrix.

Bath temperature	Reynolds number range	Mass flow rate measurements	Temperature measurements
25 °C	$596 \leq Re \leq 2\,414$	50	4 000
30 °C	$596 \leq Re \leq 2\,403$	50	4 000
35 °C	$601 \leq Re \leq 2\,406$	50	4 000
Total		150	12 000

tube length in the last section, which caused the local Nusselt numbers to increase. Therefore, the results obtained in section 5 and the last two thermocouple stations of section 4 were omitted for the 35 °C results during the analysis.

3. Data reduction

The general data reduction method used in this study was based on the UHF approach presented by Everts and Meyer [39], while the calculation of the mean fluid temperatures and heat transfer coefficients [2] were adapted for a UWT boundary condition. To investigate the local heat transfer characteristics along the test section, a non-linear least squares curve fit was used to obtain the mean fluid temperatures at each measuring station along the tube length. This curve fitting method incorporated the measured fluid temperatures, along with their respective uncertainties, guided by the expected theoretical trend of the mean fluid temperatures. The wall temperatures at the end of each water bath section, where the mean fluid temperatures were recorded, were calculated using linear interpolation. This method is illustrated in Fig. 4.

The wall temperature (shown in orange in Fig. 4) at each thermocouple station was determined by taking the average of the three temperature measurements from the thermocouples:

$$T_{w,n} = \frac{T_{w1,n} + T_{w2,n} + T_{w3,n}}{3} \tag{15}$$

Because of the high thermal conductivity of the copper test section (401 W/m.K), the temperature difference across the tube wall was assumed to be negligible. Therefore, it was assumed that the wall temperatures measured by the thermocouples fixed into the indentations in the tube wall were the same as the wall temperatures inside the test section.

The wall temperature at the end of each section (shown in green in Fig. 4) was obtained by linearly interpolating between the last wall temperature in the specific section and the first in the next section:

$$T_{w,n} = T_{w,n-2} + (x_{o,n} - x_{n-1})\left(\frac{T_{w,n-1} - T_{w,n-1}}{x_{n-1} - x_{n-2}}\right) \tag{16}$$

The wall temperature at the end of the last section was obtained by linearly extrapolating the measurements of the last two thermocouple stations:

$$T_{w,e} = T_{w,e-2} + \left(\frac{T_{w,e-1} - T_{w,e-2}}{x_{e-1} - x_{e-2}}\right)(x_{o,5} - x_{e-2}) \tag{17}$$

As the wall-fluid temperature difference decays exponentially along the test section for UWT flow [2], the mean fluid temperature along the tube, $T_f(x_n)$, was approximated using the function (shown in red in Fig. 4):

$$T_f(x_n) = f(x_n) = \sum_{i=1}^{M} c_i \varphi_i(x_n) = c_1\varphi_1(x_n) + c_2\varphi_2(x_n) = c_1 + c_2 e^{c_3 x_n} \tag{18}$$

Two basis functions, denoted as $\varphi_1(x)$ and $\varphi_2(x)$ were used for the non-linear least squares curve fit. The first basis function $\varphi_1(x)$ was assigned a constant value of 1, while the second basis function, $\varphi_2(x)$ was selected as an exponential function. These choices of basis functions were made to represent the anticipated theoretical trend of the mean fluid temperature profile. The theoretical mean fluid temperature

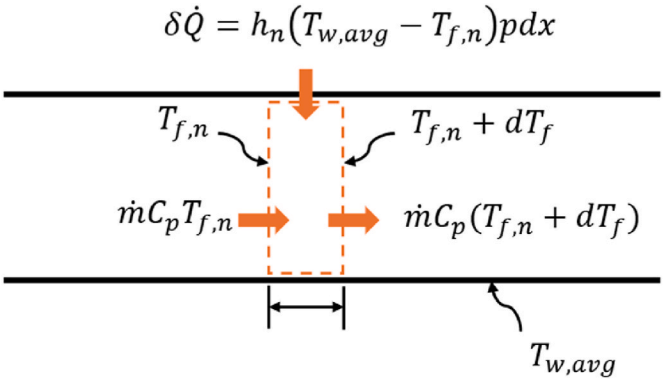

Fig. 5. Schematic of the steady-flow energy interactions on a control volume representing a tube slice with a thickness *dx*. Figure adapted from Çengel and Ghajar [2].

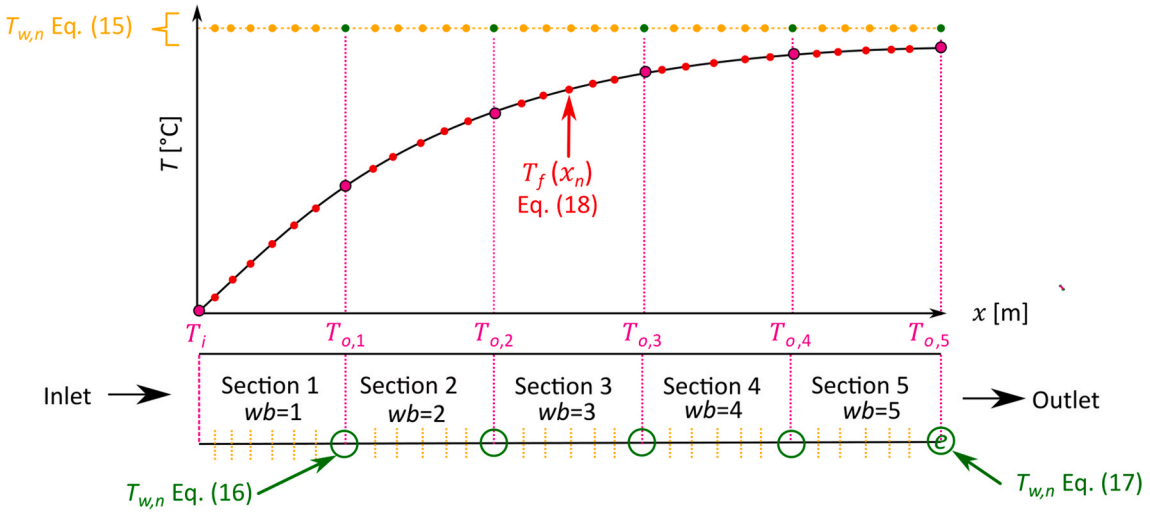

Fig. 4. Schematic summary of the measured wall temperatures (orange) fluid temperatures predicted using a non-linear least squares curve fit (red), linearly interpolated wall temperatures (green) and measured fluid temperatures (pink).

profile, derived from considering an energy balance on a control volume of thickness dx (shown in Fig. 5), follows the formulation by Çengel and Ghajar [2] and is given as:

$$T_f(x_n) = T_w - (T_w - T_i)e^{-\frac{hpx}{\dot{m}C_p}} \tag{19}$$

The form of the model used to predict the mean fluid temperature matches the form of the theoretical mean fluid temperature profile. The coefficient c_1 was adjusted to ensure that as x tends towards infinity, the mean fluid temperature tends to the wall temperature. The exponential basis function included two coefficients: c_2, governing the amplitude of the exponential curve, and c_3, determining the rate of exponential growth or decay. Notably, the parameters c_3 and c_2 were always negative, which corresponds to the expected exponential decaying trend seen from the theoretical mean fluid temperature profile.

The value of the coefficients was obtained through an optimisation algorithm, the 'nlinfit' function from Octave, which minimised the sum of squared errors by adjusting the coefficients. The errors were defined as the differences between the predicted values from the model (representing the approximated mean fluid temperature) and the actual measured mean fluid temperatures at the inlet and outlet of each water bath section. This non-linear least squares curve fit enabled the determination of coefficients that best fit the observed data, enhancing the accuracy of the temperature modelling process.

As schematically illustrated in Fig. 5, the local heat transfer coefficient (h_n) at each measuring station was determined using a steady-flow energy balance applied to a control volume representing a slice of the tube with a thickness dx [2].

The local heat transfer coefficient (h_n) was calculated from the steady-flow energy balance:

$$h_n = \frac{\dot{m}C_p}{p\,(T_{w,avg} - T_{f,n})}\left.\frac{dT_f}{dx}\right|_n \tag{20}$$

The slope of the mean fluid temperature (dT_f/dx) was determined using a central differencing approach for each point along the tube:

$$\left.\frac{dT_f}{dx}\right|_n = \frac{T_{f,n+1} - T_{f,n-1}}{x_{n+1} - x_{n-1}} \tag{21}$$

The slope of the mean fluid temperature was calculated by considering three points, therefore, the wall temperature was determined from the average of the corresponding three points:

$$T_{w,avg} = \frac{T_{w,n+1} + T_{w,n} + T_{w,n-1}}{3} \tag{22}$$

All fluid properties were determined using the thermophysical correlations developed by Popiel and Wojtkowiak [40] for water as a function of temperature. The local fluid properties were determined using the mean fluid temperature that was calculated using Eq. (18). After the local heat transfer coefficient had been determined, the local Nusselt number (Nu) was calculated as:

$$Nu = \frac{h_n D}{k_n} \tag{23}$$

The average heat transfer coefficient was calculated by using the logarithmic mean temperature difference:

$$h_{avg} = -\left[ln\left(\frac{T_{w,avg} - T_e}{T_{w,avg} - T_i}\right)\right]\frac{\dot{m}C_p}{A_w} \tag{24}$$

After the average heat transfer coefficient had been determined, the average Nusselt number (Nu_{avg}) was calculated as:

$$Nu_{avg} = \frac{h_{avg} D}{k_b} \tag{25}$$

The average wall and fluid temperatures were obtained through numerical integration. The average fluid properties for water were determined at the bulk fluid temperature calculated using the trapezoidal rule:

$$T_b = \frac{1}{L(x)}\int_0^{L(x)} T_{f,n}(x)dx \tag{26}$$

The local and average non-dimensional parameters were calculated using the mean fluid temperature and the bulk fluid temperature, respectively. The Reynolds numbers (Re) and Grashof numbers (Gr) were calculated as follows:

$$Re = \frac{\dot{m}D}{\mu A_c} \tag{27}$$

$$Gr = \frac{g\beta(T_w - T_f)D^3}{\nu^2} \tag{28}$$

The ambient temperature of the laboratory where the experiments were conducted was susceptible to environmental temperature changes, and the maximum ambient temperature change during the entire testing period was 15 °C. Therefore, to ensure consistency across all experiments, the fluid and wall temperatures were normalised using the initial inlet fluid temperature measured when testing a specific bath temperature and Reynolds number combination. This normalisation process not only ensured coherence between tests, but also enabled the amalgamation of results from tests using different bath sections into a unified data point. Across the entire dataset, the maximum and average inlet temperature variation observed was only 0.91 °C and 0.36 °C, respectively. Furthermore, a review of the results showed that the local Nusselt numbers calculated between the transition of sections 1-2 and 3-4 misrepresented the overall Nusselt number profile due to inadequate mixing at the junction between these sections. To best represent the Nusselt profile trends, the thermocouple stations at x/D = 192, 205, 600 and 612 were omitted.

The UHF uncertainty analysis calculations presented by Everts and Meyer [39] were adapted for a UWT boundary condition. The method suggested by Dunn [41] was implemented to determine the uncertainties associated with the parameters derived from the data reduction, while the method of Moffat [42] was followed to obtain the uncertainties of the non-linear least squares curve fit coefficients which was used to predict the mean fluid temperatures. The uncertainties were computed within a 95 % confidence interval.

The uncertainties of the predicted mean fluid temperatures from the model were computed by assessing the uncertainty of each model coefficient and incorporating the uncertainty of the measured mean fluid temperatures. Therefore, 1 000 samples of the measured mean fluid temperatures were generated by introducing random noise to the measurements of which the magnitude corresponded to the respective uncertainty. Subsequently, the optimisation routine was executed on these samples to deduce the three coefficients, resulting in three sets of 1 000 samples, and the variance of the samples for each coefficient accounted for the uncertainty of the measured mean fluid temperatures. The mean value of the coefficients across the samples was then used as the coefficient value, and the uncertainty of each coefficient was determined by calculating the standard error of the mean.

The uncertainty analysis determined that the average local Nusselt number uncertainties were 19.1 %, 9.9 %, and 7.9 % for bath temperatures of 25 °C, 30 °C, and 35 °C, respectively, while the average local Grashof number uncertainties were 15.3 %, 9.6 %, and 7.9 % at the same bath temperatures. Both the local Nusselt number and Grashof number uncertainties increased along the tube length, as well as with decreasing bath temperatures, due to the decreasing wall-fluid temperature differences. The average Reynolds number uncertainty for all three bath temperatures was 4.7 %, and the average Nusselt number uncertainties were 4.0 %, 3.7 %, and 3.7 % for bath temperatures of 25 °C, 30 °C, and 35 °C, respectively.

4. Validation

4.1. Average Nusselt numbers

As will be shown in Fig. 8, the average wall temperature along the tube length was lower than the outlet fluid temperature, because the wall temperature did not remain constant along the test section. Therefore, when calculating the average heat transfer coefficient, as shown in Eq. (24), it was not possible to use the logarithmic mean temperature difference along the entire test section. Instead, the average Nusselt numbers were calculated by only considering the tube length for which the average wall temperature was greater than the outlet fluid temperature. Therefore, the last portion of the test section, which contained very small wall-fluid temperature differences, were omitted in this analysis. This approach allowed for the use of Eq. (24) to calculate the average Nusselt numbers similar to previous studies. The average Nusselt numbers along the tube length were compared to the correlations proposed by Depew and August [18] (Eq. (4)), Yousef et al. [19] (Eq. (5)) and Gnielinski [32] (Eq. (11)) in Fig. 6. It is of note that the experimental correlations developed by Jackson et al. [15], Oliver [16], and Brown and Thomas [17] were not used, because their larger Grashof number ranges misrepresented the Nusselt number trends. The Grashof number range for this study was between 28 and 2 540, while the lower Grashof number limit for those correlations for water is 2.9×10^4.

The results correlated very well with the experimentally developed correlation of Depew and August [18], with an average deviation of 3.8 % between Reynolds numbers of 600 and 2 000, while the average deviation from the experimentally developed correlation of Yousef and Tarasuk [19] was 7.4 % between Reynolds numbers of 600 and 2 000. The analytical correlation of Gnielinski [32] had an average deviation of 9.4 %. A general trend in this figure was that the Nusselt numbers were greater than the theoretical Nusselt number of 3.66 for fully developed forced convective laminar UWT flow and that it increases with Reynolds number. This indicative that mixed convection conditions existed, which is analysed in detail in Section 6.1.

It also follows from Fig. 6 that the Nusselt numbers rapidly increased for Reynolds numbers greater than 2 000. This indicates that the transitional flow regime started sooner than the generally assumed Reynolds number of 2 300 [2]. This is not unexpected, as Everts and Meyer [28] found that the critical Reynolds number is significantly affected by several factors, including the tube diameter and free convection effects.

4.2. Local Nusselt numbers

To validate the local Nusselt numbers, the experimental data at a Reynolds number of 1 000 and a bath temperature of 30 °C was compared to the correlations proposed by Churchill and Ozoe [29] (Eq. (6)), Gnielinski [32] (Eq. (10)) and Bennet [33] (Eq. (14)) in Fig. 7. The dotted black line indicates the theoretical Nusselt number of 3.66 for fully developed forced convective laminar flow through a circular tube with a UWT boundary condition [2]. Although these correlations do not account for free convection effects, to the authors' best knowledge, no correlations were available to predict the local heat transfer coefficients and local Nusselt numbers of mixed convective laminar UWT flow for the ranges used in this study.

From the error bars in Fig. 7, it follows that the uncertainties were low near the inlet but then increased along the length due to the decreasing wall-fluid temperature difference. The experimental data had an average deviation of 36.0 %, 39.1 % and 43.4 % when compared to those of Churchill and Ozoe [29], Gnielinski [32], and Bennet [33], respectively. The Nusselt numbers correlated well near the inlet of the test section, but due to the presence of free convection effects, deviated further along the tube length and became approximately constant for $x/D > 250$. The increased Nusselt numbers compared to the theoretical forced convective Nusselt number of 3.66 was because mixed convection conditions existed, and this is investigated in more detail in Section 6.2.

5. Wall temperature uniformity

5.1. Local wall temperature

This study aimed to experimentally obtain a UWT boundary condition for water flowing through a horizontal tube. The wall temperature uniformity was evaluated in Fig. 8 by comparing the wall temperature measurements taken at each increasing bath length for a given bath temperature of 35 °C and Reynolds number of 800. Also included in this graph are the measured (hollow circle markers) and predicted mean fluid temperatures (dotted black line). It follows from this figure that although repeatable results were obtained for different bath lengths, the measured wall temperatures were not uniform along the test section. Instead, the wall temperature gradually increased for $x/D < 600$ before becoming approximately constant. Despite these local wall temperature non-uniformities, the notable correlation of the average Nusselt numbers with literature in Fig. 6 suggests that other studies experienced similar non-uniformities. The studies summarised in Table 1 also reported some variations in the wall temperatures, despite their test sections being significantly shorter than in this study. Therefore, those wall temperature non-uniformities might have been even more pronounced if they used longer test sections. To the authors' best knowledge, previous experimental studies did not specifically analyse the local wall temperatures along the tube length to investigate any non-uniformities or trends. Therefore, there is uncertainty about the actual wall temperature uniformities when experimentally investigating UWT flow.

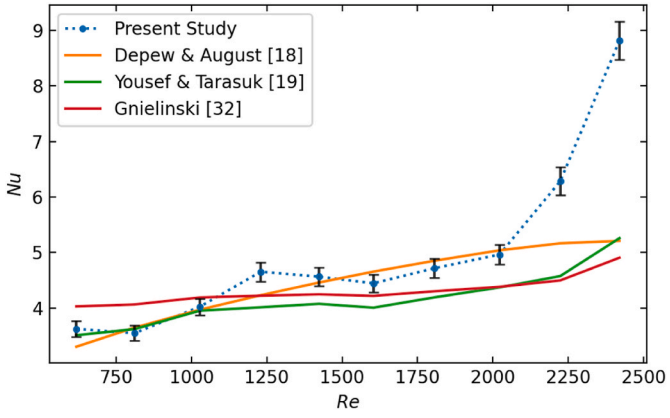

Fig. 6. Comparison of the average Nusselt numbers as a function of Reynolds number with literature at a bath temperature of 30 °C.

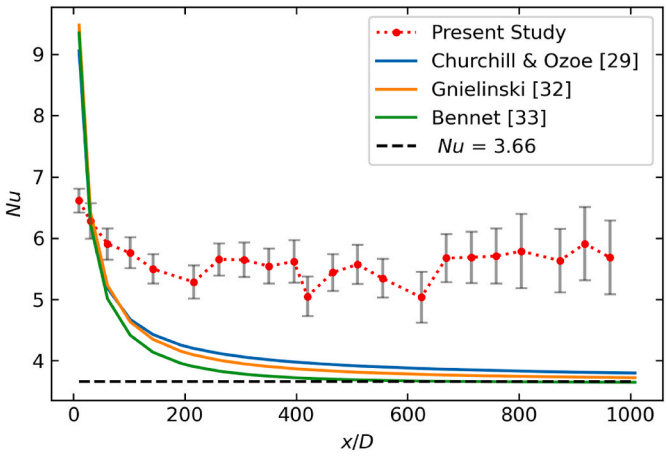

Fig. 7. Local Nusselt numbers as a function of axial position compared to literature at a bath temperature of 30 °C and at a Reynolds number of 1 000.

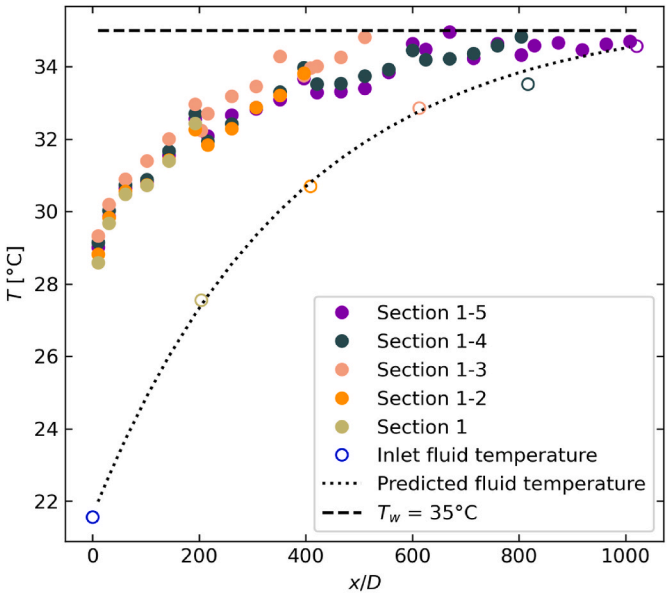

Fig. 8. Wall temperatures (solid circle makers) measured fluid temperatures (hollow circle makers) and predicted fluid temperatures (dotted black line) as a function of axial position compared for different bath lengths at a bath temperature of 35 °C and a Reynolds number of 800.

As illustrated in Fig. 9, the cause of the non-uniformity is most likely due to the heat transfer coefficients in the water bath being lower than that inside the test section. For developing flow, the maximum heat transfer coefficients are found at the inlet of the test section and then they gradually decrease along the tube length as the flow develops. Therefore, the high developing heat transfer coefficients inside the tube dominated the heat transfer coefficients inside the water bath (thus outside the tube). This caused the wall temperatures to decrease (because the temperature of the fluid inside the test section was lower than in the bath) and deviate from the temperature in the water bath. According to Celata [43], macro-scale heat transfer is generally assumed to take place in the radial direction only. Therefore, axial heat conduction was neglected as the axial heat conduction number [44] for the results presented in this study did not exceed 0.002.

The internal thermal resistance (R_f) is smaller than the external thermal resistance (R_{bath}) due to the higher internal heat transfer coefficient when the flow is developing. Therefore, the heat transfer to the copper tube wall was dominated by the internal fluid temperature. The wall thermal resistance (R_{wall}) was considered to be negligible, due to the tube's higher thermal conductivity and small wall thickness. As the flow developed along the tube length, the internal heat transfer coefficients decreased, and the external heat transfer coefficients became dominant, which explains why the deviation from the water bath temperature decreased along the tube length. It is worth noting that

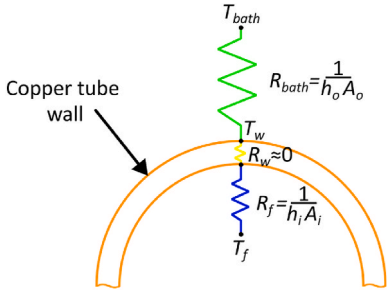

Fig. 9. Schematic of the thermal resistances and heat transfer path through a cross section of the test section near the inlet of the tube.

although higher external heat transfer coefficients could have been obtained when using wet steam (vapour) to achieve a UWT boundary condition, this would have been increasingly complicated in this study due to the multi-section water bath approach that was followed to measure the mean fluid temperatures along the tube length. Being able to measure the mean fluid temperatures was vital to investigate the local heat transfer characteristics and therefore, as discussed in Section 2, care was taken to ensure control of the temperature and flow to each bath section.

5.2. Effect of bath temperature

The extent to which the bath temperature affected the wall temperature uniformity was investigated in Fig. 10 by comparing the wall temperatures measured at a Reynolds number of 800 for different bath temperatures and an average inlet fluid temperature to the test section of 21.2 °C. From this figure, it follows that as the bath temperature (and thus the temperature difference between the test fluid and bath) increased, the wall temperature non-uniformity increased. Furthermore, when increasing the temperature difference between the bath and the inlet fluid temperature to the test section, both the gradient of the wall temperatures as well as the axial distance before becoming constant, increased. The wall temperatures increased for $x/D < 200$, $x/D < 600$ and $x/D < 800$ for bath temperatures of 25 °C, 30 °C and 35 °C, respectively, before becoming approximately constant. As these trends are caused by the wall-fluid temperature differences, similar trends can be expected when considering a fixed wall temperature and varying the inlet fluid temperature to the test section.

Four of the six studies summarised in Table 1 had an inlet wall-fluid temperature difference greater than 20 °C with two studies [15,19] exceeding 50 °C. Therefore, previous studies might have experienced similar or even worse wall temperature non-uniformities. Furthermore, the longest non-dimensional tube length used was 110, which is less than the tube length required for the wall temperature to become constant at 25 °C in this study (based on the wall temperature profile in Fig. 8). This further supports the possibility that wall temperature non-uniformities existed in previous studies and that developing flow rather than fully developed flow was investigated.

5.3. Effect of Reynolds number

It followed from Section 5.1 that the wall non-uniformity was significantly influenced by the high internal heat transfer coefficient at the inlet of the tube. Since the thermal entrance length is a function of the Reynolds number [2], it can be expected that the Reynolds number

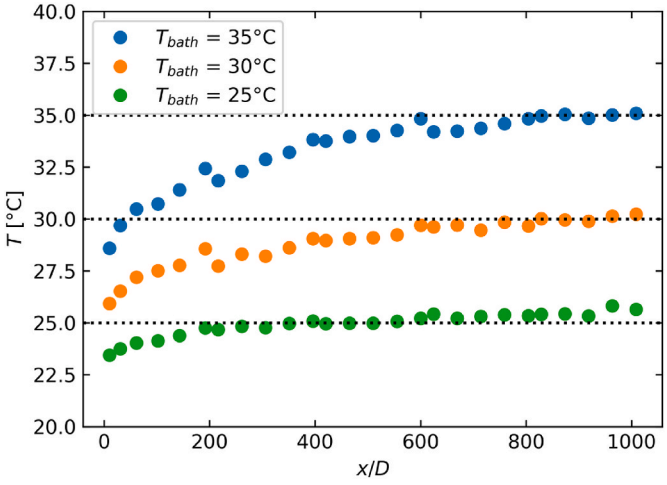

Fig. 10. The local wall temperatures compared for different bath temperatures at a Reynolds number of 800 and an average inlet fluid temperature of 21.2 °C.

will also affect the wall temperature uniformity. This was investigated by comparing the wall temperatures measured at various Reynolds numbers at a set bath temperature of 35 °C in Fig. 11. This figure indicates that the magnitude of the wall temperatures decreased with increasing Reynolds number, but the non-uniformities of the wall temperatures increased. This was due to the increasing internal heat transfer coefficients, associated with increasing Reynolds numbers, dominating the external heat transfer coefficient. Furthermore, the axial position where the wall temperature became approximately constant increased with increasing Reynolds number. The thermal entrance length is proportional to the Reynolds number, which confirms that the non-uniformities were caused by the developing flow inside the test section. A uniform wall temperature can therefore only be expected at lower Reynolds numbers, when the thermal entrance length is short in comparison to the overall tube length and the flow becomes fully developed earlier along the tube length, or when having small wall-fluid temperatures as indicated in Fig. 10. It is of note that the general trend of the wall temperatures is similar to the mean fluid temperature trend in Fig. 8, indicating that there is a relationship between developing flow and the wall temperature non-uniformities.

5.4. UWT assumption

It was shown in Fig. 6 that despite the wall temperature non-uniformities, the experimental data correlated well with those of Depew and August [18] and to a lesser extent to Yousef and Tarasuk [19]. This suggests that, although not explicitly reported, these studies experienced similar wall temperature non-uniformities. The effect of the wall temperature non-uniformities on the local and average Nusselt numbers was investigated in Fig. 12 by replacing the measured wall temperatures with a constant wall temperature equal to the maximum wall temperature measured.

As this satisfied the criterion for a UWT boundary condition, it was expected that the subsequent results would improve. However, it follows from Fig. 12(a) that the average Nusselt numbers could no longer be predicted using the correlation of Depew and August [18] or Yousef and Tarasuk [19]. The significant difference between Fig. 12(a) and Fig. 6 suggests that the correlations also involved wall temperature non-uniformities and it can be postulated that other experimentally developed correlations also contained wall temperature non-uniformities. This indicates that achieving a perfect UWT experimentally is more challenging than expected and raises the question if it is possible at all for developing flow.

Furthermore, the red data in Fig. 12(b) indicates that when assuming a constant wall temperature, the local Nusselt numbers no longer followed the predicted trends and were underpredicted with an average deviation of 26.4 % and 35.2 %, when compared to the Nusselt numbers

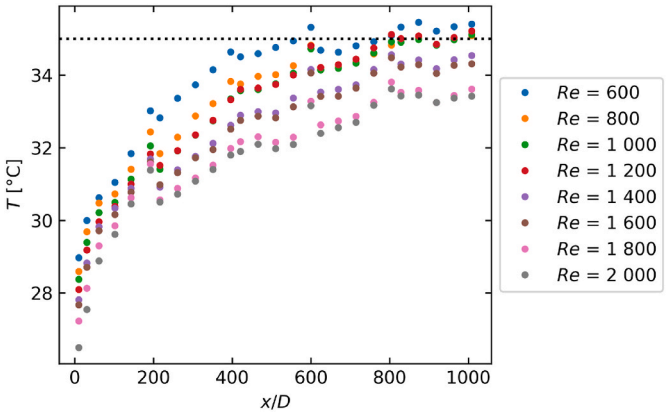

Fig. 11. The local wall temperatures compared at different Reynolds numbers for a bath temperature of 35 °C.

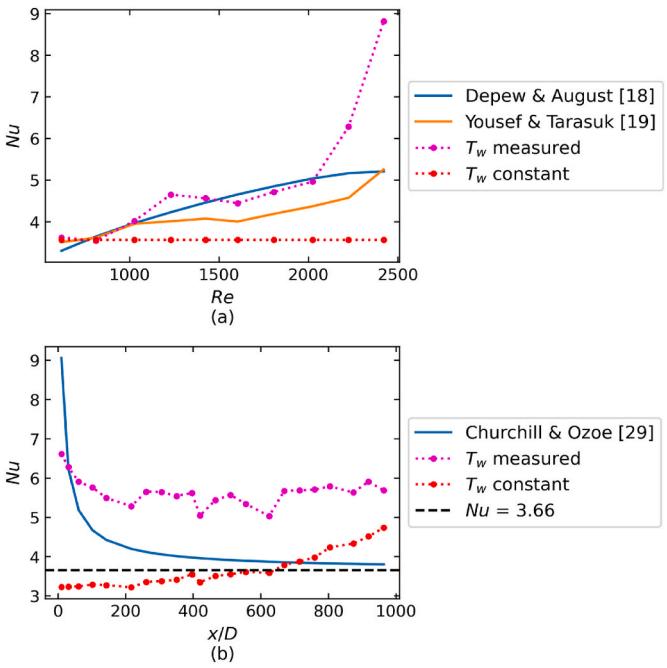

Fig. 12. Comparison of (a) average Nusselt numbers and (b) local Nusselt numbers at a Reynolds number of 1 000, calculated assuming a constant wall temperature of 30 °C, as well as the Nusselt numbers calculated using measured wall temperature at a bath temperature of 30 °C.

predicted by Churchill and Ozoe [29] and those calculated from the measured wall temperatures, respectively. This deviation of the local Nusselt numbers with a true UWT boundary condition indicates possible discrepancies between the results obtained from analytical and experimental studies. These findings also indicate that the wall temperature non-uniformities might not void the assumption of UWT flow but could be an integral part of experimentally investigating developing UWT flow.

6. Heat transfer results

6.1. Mixed convective developing flow

Everts and Meyer [22] noted that most heat exchangers operate with mixed convective flow due to the temperature and density differences in the presence of gravity. The cross-sectional temperature gradients lead to the creation of two symmetrical vortices in the cross-section and a helical or corkscrew-like motion along the tube length. Recent numerical studies [10,21] investigated developing laminar UHF flow and showed how the heat transfer and flow characteristics change along the tube length for both forced and mixed convective flow. The additional fluid motion present in mixed convective flow compared to forced convective flow, enhances mixing and heat transfer, but also affects the development of the hydrodynamic and thermal boundary layers [22]. Oliver [16] also showed that mixed convection can increase the heat transfer rate by a factor of three of four. Therefore, it is important to determine whether free convection effects can be neglected or not.

A flow regime map is a valuable tool to help determine whether free convection effects are significant. Metais and Eckert [45] developed a flow regime map for UWT flow and considered the flow to be mixed convective when the Nusselt numbers exceeded the corresponding forced convective Nusselt numbers by 10 %. The same criterion was used by Everts and Meyer [9] for their UHF flow regime maps. Metais and Eckert [45] also noted that the development of a UWT flow regime map was made exceedingly difficult owing to the lack of UWT experimental publications. Despite these uncertainties, as well as the results of

this study being outside their suggested range of $10^{-2} < PrD/L < 1$, the UWT flow regime map of Metais and Eckert [45] has been used in Fig. 13 as a guideline to determine whether the experimental results can be expected to contain mixed convective flow.

Fig. 13 suggests that all the experimental results fell in the forced convection (FC) laminar flow regime. However, as shown in Fig. 7, the local Nusselt numbers deviated from the forced convection correlations after $x/D = 102$ and did not continue to decrease but were higher than those predicted by forced convective correlations due to the presence of free convection effects. Everts and Meyer [9] also noted that the UHF flow regime map of Metais and Eckert [45] predicted all their experimental results as forced convective despite 95 % of the results being dominated by mixed convection.

The presence of free convection effects can be identified by the heat transfer enhancement compared to forced convective flow. This was investigated in Fig. 14 by comparing the ratio of the experimental local Nusselt numbers to those predicted using the forced convective correlation of Gnielinski [32]. Since the local Nusselt number correlation of Gnielinski [32] accounts for forced convective developing UWT flow, this ratio would indicate the possible heat transfer enhancements caused by free convection effects. Heat transfer enhancements of up to 80 % were observed in Fig. 14, which suggests mixed convective flow. The experimental Nusselt numbers surpassed the forced convection results shortly after the inlet of the tube, indicating that free convection effects quickly developed and became significant as the thermal boundary layer developed. Thereafter, for Reynolds numbers greater than 800, the Nusselt number ratio continues to increase before approaching an asymptotic value for $x/D > 700$.

Of interest is that for Reynolds numbers of 600 and 800, the ratio increased but then decreased, indicating that the free convection effects have diminished due to the decreasing wall-fluid temperature difference along the test section (as shown in Fig. 8). For a Reynolds number of 800, the Nusselt number approached unity, which is indicative of forced convective conditions. However, for a Reynolds number of 600, the Nusselt number ratio decreased rapidly below unity. This was not only due to the absence of free convection effects after the initial peak, but also due to fluid temperatures approaching the wall temperatures asymptotically and therefore the wall-fluid temperature differences and heat transfer diminished. This is investigated in Fig. 15 by considering the wall-fluid temperature differences (Fig. 15(a)) and local Grashof numbers (Fig. 15(b)) along the tube length for different Reynolds numbers.

For a UWT boundary condition, the theoretical trend is that the wall-fluid temperature difference decays exponentially along the tube length as the fluid temperature asymptotically approaches the uniform wall temperature. As the Grashof number, which can be used to quantify free convection effects, is a strong function of the wall-fluid temperature difference, it can also be expected to decay exponentially along the tube length. However, it follows that, for mixed convective flow, neither the wall-fluid temperature differences nor the Grashof numbers decayed exponentially along the tube length.

Fig. 15(a) indicates that the wall-fluid temperature difference initially increased as the thermal boundary layer and free convection effects developed, which is confirmed by the increasing Grashof numbers in Fig. 15(b), and explains the increasing Nusselt number ratios in Fig. 14. At a fixed Reynolds number of 1 600, the wall-fluid temperature differences peaked around $x/D = 62$ for all three bath temperatures, while the Grashof numbers only peaked at around $x/D = 142$. The difference in axial positions at which the peaks occurred were due to the combined effects of developing flow and free convection effects, both developing from the inlet of the tube. As the thermal boundary layer started developing from the tube inlet, free convection effects increased. However, the wall-fluid temperature differences decreased along the tube length after the initial peak. The Grashof number peak

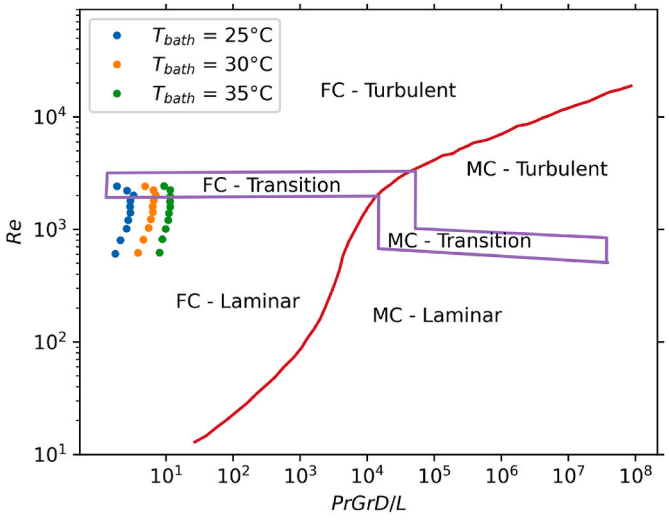

Fig. 13. Experimental data of this study plotted on the flow regime map of Metais and Eckert [45] for UWT flow in horizontal tubes.

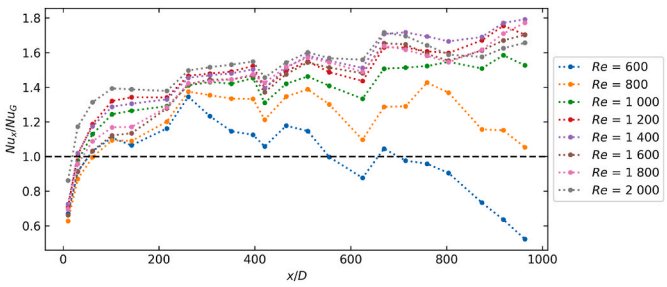

Fig. 14. The ratio of the experimental local Nusselt numbers to those calculated by the forced convection correlation of Gnielinski [32] at a bath temperature of 30 °C as a function of axial position.

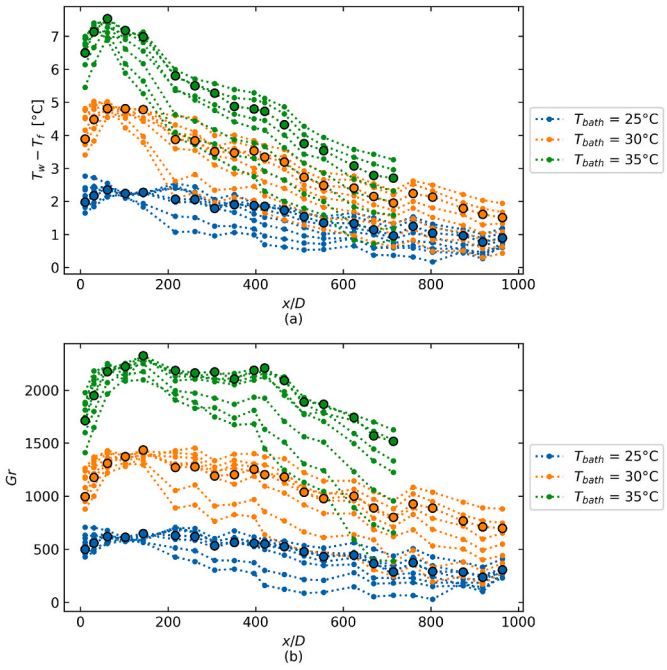

Fig. 15. Comparison of (a) wall-fluid temperature difference and (b) local Grashof numbers as a function of axial position for bath temperatures of 25 °C, 30 °C and 35 °C for Reynolds numbers between 600 and 2 000. The black circle markers indicate results at a Reynolds number of 1 600.

being later than for the wall-fluid temperature differences, is indicative that the thermal boundary layer and free convection effects were still developing despite the decreasing wall-fluid temperature differences. Although the maximum wall-fluid temperature difference in this study was less than 8 °C, the cross-sectional temperature variations were sufficient to lead to mixed convective flow. Furthermore, as the bath temperature was increased, the magnitude of the wall-fluid temperature differences and Grashof numbers increased, allowing for greater free convection effects [17].

After the peaks, both the wall-fluid temperature differences and Grashof numbers decreased, which indicated that the decreasing wall-fluid temperature differences dominated and prevented free convection effects from developing further. Oliver [16] also noted decreasing free convection effects caused by the decreasing wall-fluid temperature gradients. The gradient of both the wall-fluid temperature differences and Grashof numbers became steeper for increasing bath temperatures and Reynolds numbers. It is also worth noting that the gradient of wall-fluid temperature differences was always steeper than for the Grashof numbers and that the variation of Grashof numbers for different Reynolds numbers was less than the variation in the wall-fluid temperature differences. This indicates that although the Grashof number is a function of the wall-fluid temperature difference, the secondary fluid motion caused by the presence of free convection effects assisted in preserving free convection effects which dampened and delayed the associated decrease caused by the diminishing wall-fluid temperature differences.

From close inspection of the trends in Fig. 15(a) and (b), it was found that a change in gradient occurred at approximately $x/D = 760$ for a Reynolds number of 1 600 and bath temperature of 30 °C. This trend became more distinct when the bath temperature was increased to 35 °C and also occurred earlier along the tube length. Free convection effects therefore experienced a self-diminishing effect. As can be seen from Fig. 15(b), the Grashof number and thus free convection effects increased with bath temperature, which lead to higher heat transfer rates and therefore, the fluid temperatures approached the wall temperatures faster. However, the rapidly decreasing wall-fluid temperature differences caused free convection effects and secondary flow to decrease rapidly as the flow approached fully developed flow. This is in good agreement with the findings of Everts and Meyer [22] that free convection effects assist with the development of the thermal boundary layer.

It also follows from Fig. 15 that at a bath temperature of 25 °C, the wall-fluid temperature differences and Grashof numbers became approximately constant at $x/D = 804$. The small wall-fluid temperature differences of approximately 0.6 °C indicate very low heat transfer rates. At a bath temperature of 30 °C, the wall-fluid temperature differences and Grashof number became approximately constant at $x/D = 874$ for a Reynolds number of 1 600 and at approximately $x/D = 712$ for the lowest Reynolds number of 600. When comparing this to the Nusselt number ratio in Fig. 14, it corresponds to the axial position where the ratio decreased below unity for a Reynolds number of 600. This indicates that heat transfer diminished due to very small wall-fluid temperature differences.

6.2. Local Nusselt numbers

To investigate the trends of the local Nusselt numbers through tubes exposed to a UWT boundary condition, Fig. 16(a) compares the local Nusselt numbers for different Reynolds numbers at a bath temperature of 30 °C. Furthermore, for clarification purposes, the corresponding wall-fluid temperature differences and local Grashof numbers are compared in Fig. 16(b) and (c). From this figure it follows that, for a Reynolds number of 1 600, the local Nusselt numbers experienced an initial decrease from the inlet to a minimum at $x/D = 142$, then subsequently increased and were approximately constant for $x/D > 260$. The trough represents the axial position at which free convection effects

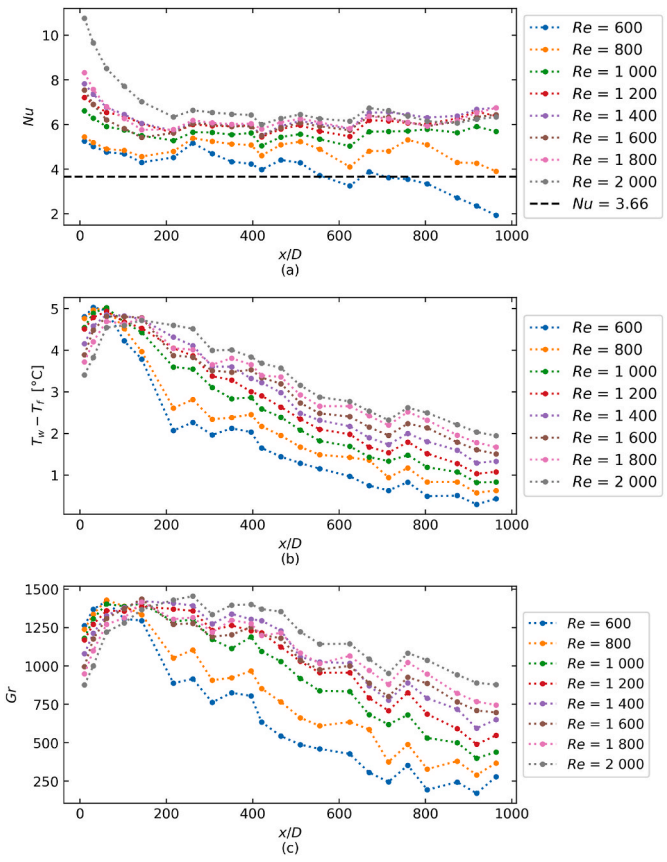

Fig. 16. Comparison of (a) local Nusselt numbers, (b) local wall-fluid temperatures, and (c) local Grashof numbers as a function of axial position for different Reynolds numbers at a bath temperature of 30 °C.

started dominating entrance effects and this corresponded with the peaks in the local Grashof number (black highlighted orange data points in Fig. 15(b)), thus the point where maximum free convection effects could be expected. Although free convection effects began to decrease after this point (due to the decreasing wall-fluid temperature differences), they were sufficient to enhance mixing and thus heat transfer, compared to forced convective flow. This heat transfer enhancement was sufficient to dominate the decreasing trend of forced convective flow and cause a slight increase in local Nusselt numbers, although it existed only for a short tube length.

The subsequent plateau in the local Nusselt numbers indicates that although free convection effects decreased along the tube length, as indicated by the local Grashof numbers (Fig. 16(c)), due to the decreasing wall-fluid temperature differences (Fig. 16(b)), the secondary fluid motion assisted in dampening their decrease and sustaining their effect. The Nusselt numbers did not converge to the theoretical fully developed Nusselt number of 3.66 but became constant at higher Nusselt numbers that increased with increasing Reynolds number. As indicated in Fig. 16(b) and (c), free convection effects increase with increasing Reynolds number, which explains why the magnitude of the Nusselt numbers in Fig. 16(a) also increased. It should also be noted that the approximately constant Nusselt numbers do not necessarily indicate fully developed flow for an infinitely long tube, but rather constant local Nusselt numbers due to sustained free convection effects and sufficient wall-fluid temperature differences. The flow is generally considered to be fully developed when the fluid temperature profile becomes independent of axial position [2]. For UWT flow, the wall-fluid temperature difference decays exponentially along the tube length and it is postulated that after the fluid thermal profile and local Nusselt numbers became independent of axial position, the local Nusselt numbers

eventually decrease when the wall-fluid temperature difference is no longer sufficient for noteworthy convective heat transfer, as observed at lower Reynolds numbers in Fig. 16(a).

This explains the difference in trends between Reynolds numbers of 600 and 800 compared to higher Reynolds numbers, especially when considering the length of the test section. Fig. 16(b) indicate that the wall-fluid temperature differences continued to decrease along the tube length, which ultimately led to decreasing Grashof numbers. At the minimum Reynolds number of 600, free convection effects were minimal due to the flow approaching fully developed flow earlier along the tube length (because the thermal entrance length is proportional to Reynolds number). Due to the smaller entrance length, free convection effects developed quickly near the inlet of the tube but were not sufficient to lead to significant secondary flow to assist in sustaining them further along the tube length. Furthermore, as the tube length was sufficient for the fluid temperatures to approach the wall temperatures, the negligible wall-fluid temperature differences caused heat transfer to diminish along the tube length, and the Nusselt numbers began to decrease.

A similar transition has been reported by Yousef and Tarasuk [19] and Everts et al. [46]. Yousef and Tarasuk [19] suggested that the decreasing Nusselt number below 3.66 was due to the flow becoming thermally stratified and conduction becoming the primary mode of heat transfer. Furthermore, Everts et al. [46] found that the Nusselt numbers for UHF downward flow in a vertical tube also decreased below the theoretical forced convective Nusselt number for low laminar Reynolds numbers and heat fluxes due to opposing flow and low heat flux suppressing free convection effects. However, since the flow is still in motion, and as long as some degree of wall-fluid temperature difference is maintained, some component of convective heat transfer will remain. Although this trend can be seen in this study for Reynolds numbers of 800 and 600 at a bath temperature of 30 °C, it recommended that future experimental studies investigate this trend for a wider range of Reynolds numbers and Grashof numbers using longer tube lengths.

6.3. Heat transfer regions for UWT flow

Building upon the insights obtained into developing mixed convective UWT flow, Fig. 17 schematically summarises the local Nusselt number trends for laminar UWT flow. The dashed red line represents the theoretical fully developed forced convective Nusselt number of 3.66 for laminar UWT flow, while the other lines indicate the influence of the Reynolds number and Grashof number for mixed convective flow. Four distinct regions were identified: (1) Free Convection Developing (FCD), (2) Free Convection Governing (FCG), (3) Sustained Free Convection (SFC), and (4) Diminishing Heat Transfer (DHT).

In the Free Convection Developing (FCD) region, free convection effects start developing together with the increasing thermal boundary layer thickness. The local Nusselt numbers decrease in this region, due to the flow being developing. However, the presence of free convection effects significantly affects the heat transfer in this region. An increase in free convection effects, due to increasing Reynolds number and Grashof number, increases the magnitude of the Nusselt numbers. Furthermore, as free convection effects also assist with the development of the thermal boundary layer, the slope of the local Nusselt numbers becomes steeper. The local Nusselt numbers reach a minimum at the axial position where free convection effects start dominating the entrance effects in the Free Convection Governing (FCG) region. In this region, the thermal boundary layer thickness is sufficient for free convection effects to enhance heat transfer significantly and dominate the entrance region effects which leads to increasing local Nusselt numbers up to a peak at the end of the FCG region. The magnitude of the peak is influenced by the Grashof number and Reynolds number, and increasing either of these results in higher free convection effects that enhance the heat transfer. However, together with the increasing thermal boundary layer thickness and increasing free convection effects, the wall-fluid temperature differences decrease along the tube length. Therefore, this region only exists for a small portion of the tube.

In the Sustained Free Convection (SFC) region, the secondary fluid motion caused by free convection effects assist in sustaining the free convection effects and the temperature profile to become fully developed, despite the decreasing wall-fluid temperature differences along

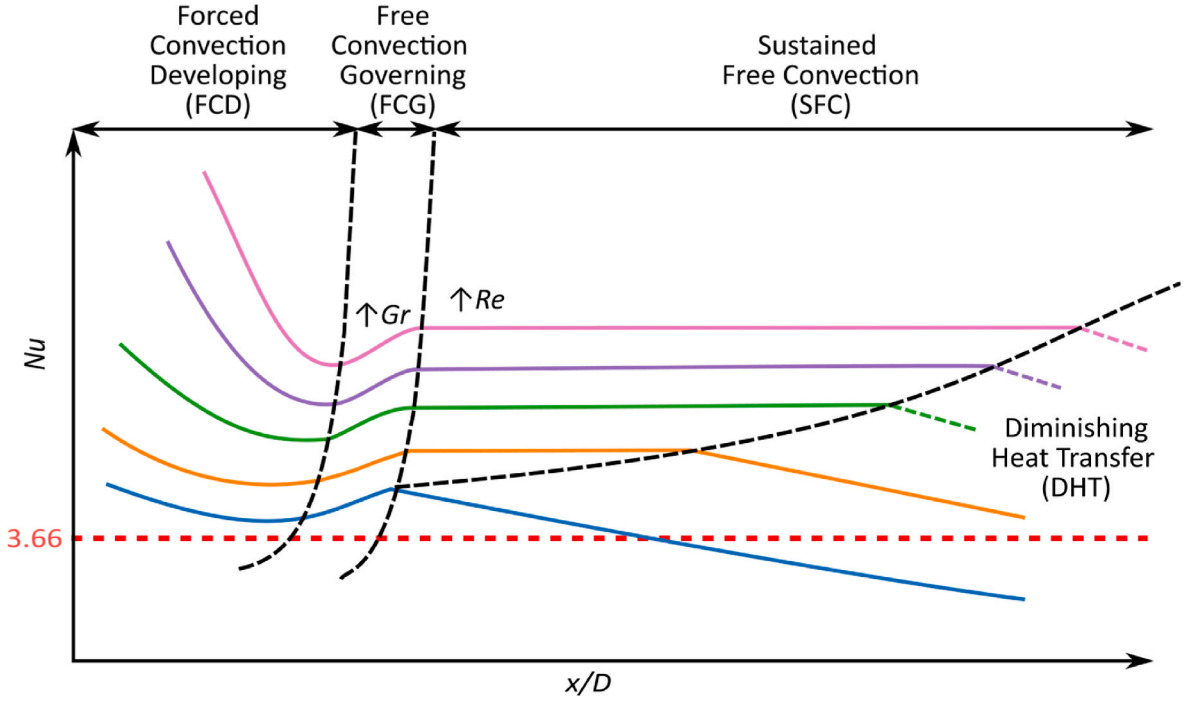

Fig. 17. Schematic of the local Nusselt number regions for laminar UWT flow, indicating the Forced Convection Developing (FCD), Free Convection Governing (FCG), Sustained Free Convection (SFC) and Diminishing Heat Transfer (DHT) regions.

the tube length. Therefore, the local Nusselt numbers remain constant along the tube length and increase in magnitude with increasing free convection effects due to increases in Reynolds number or Grashof number. However, as the wall-fluid temperature difference continually decreases and eventually diminishes along the tube length, heat transfer cannot be sustained for an infinitely long tube. Therefore, the local Nusselt numbers start to decrease in the Diminishing Heat Transfer (DHT) region and it is postulated that the Nusselt numbers will approach unity in sufficiently long tubes.

7. Conclusions

The purpose of this study was to experimentally achieve a uniform wall temperature (UWT) boundary condition and investigate the local heat transfer characteristics of developing laminar flow through a horizontal tube exposed to this boundary condition. A novel experimental setup was developed which enabled the measurement of the local mean fluid temperatures along the tube length and thus the calculation of the local heat transfer coefficients, while previous studies focused on average heat transfer coefficients only. Experiments were conducted for Reynolds numbers between 600 and 2 400 at three different bath temperatures. The findings of this study offer compelling insights into the complexities of experimentally achieving a UWT boundary condition as well as the resulting heat transfer characteristics when the flow is still developing, and mixed convection conditions exist.

Although care was taken to ensure that the temperatures inside the water bath were uniform to achieve a UWT boundary condition, the measured wall temperatures along the test section showed that wall temperature did not remain uniform, but increased from the inlet and only approached a constant value further along the test section. The reason for this trend was that the flow inside the tube was developing and the high heat transfer coefficients inside the tube dominated the external heat transfer coefficients inside the water bath. As the wall temperatures were affected by the mean fluid temperatures inside the tube, the trend of the wall and fluid temperatures along the tube length was found to be comparable. However, despite the wall temperature non-uniformities the average results correlated well with literature, indicating that previous experimental studies probably encountered similar wall temperature non-uniformities. This also highlights the difficulty and uncertainty involved in experimentally investigating UWT flow. When mathematically applying a perfect UWT, the results no longer matched the expected developing heat transfer trends, emphasising the existence of wall temperature non-uniformities and the importance of accounting for them.

Although a UWT flow regime map in literature predicted the results to be dominated by forced convection, mixed convective characteristics evident and the heat transfer coefficients were increased by upwards of 80 % when compared to forced convection correlations. In general, it was found that free convection effects increased with increasing Reynolds number and/or bath temperature, due to the higher wall-fluid temperature differences. Due to the exponentially decaying wall-fluid temperature difference along the tube length, which is associated with UWT flow, free convection effects could not be sustained along the entire tube length. The secondary fluid motion caused by these free convection effects assisted in sustaining significance of free convection effects and the local Nusselt numbers to become constant. However, free convection effects ultimately decreased and became negligible as the fluid temperature approached the wall temperature and heat transfer diminished. This resulted in decreasing Nusselt numbers at low Reynolds numbers of 600 and 800, due to the shorter thermal entrance lengths for these lower Nusselt numbers.

After analysing the local heat transfer characteristics of developing laminar flow through horizontal tubes exposed to a UWT boundary condition, four distinct regions were defined in the local Nusselt trends: (1) Free Convection Developing (FCD), (2) Free Convection Governing (FCG), (3) Sustained Free Convection (SFC), and (4) Diminishing Heat Transfer (DHT). In the Free Convection Developing (FCD) region, free convection effects start developing together with the increasing thermal boundary layer thickness. An increase in free convection effects, increases the magnitude and slope of the Nusselt numbers, although the general trend remains decreasing Nusselt numbers due to the dominating entrance effects. In the Free Convection Governing (FCG) region, the thermal boundary layer thickness is sufficient for free convection effects to enhance heat transfer significantly and dominate the entrance region effects, however, this region only exists for a small portion of the tube due to the decreasing wall-fluid temperature differences. In the Sustained Free Convection (SFC) region, the secondary fluid motion caused by free convection effects assist in sustaining the free convection effects and the local Nusselt numbers remain constant along the tube length, but increase in magnitude with increasing free convection. However, as the wall-fluid temperature difference exponentially decays along the tube length, the local Nusselt numbers eventually start to decrease in the Diminishing Heat Transfer (DHT) region due to diminishing heat transfer.

CRediT authorship contribution statement

Mark J. Coetzee: Writing – original draft, Visualization, Validation, Investigation, Data curation. **Deniel Steyn:** Data curation, Investigation, Methodology, Visualization, Writing – review & editing. **Marilize Everts:** Writing – review & editing, Supervision, Resources, Project administration, Methodology, Investigation, Funding acquisition, Conceptualization.

Declaration of competing interest

The authors declare that they have no known competing financial interests or personal relationships that could have appeared to influence the work reported in this paper.

Data availability

Data will be made available on request.

Acknowledgements

The funding obtained from the National Research Foundation (Grant Number: 116623), Stellenbosch University/University of Pretoria Solar Hub, and Research Development Programme at the University of Pretoria is acknowledged and duly appreciated.

References

[1] S. Nagar, P.K. Singh, A short review on the Industrial applications of phase change materials, IOP Conf. Ser. Mater. Sci. Eng. 1116 (1) (2021) 012006.
[2] Y.A. Cengel, A.J. Ghajar, Heat and mass transfer: fundamentals and applications, in: SI Units, 6 ed., McGraw-Hill Education, New York, 2020.
[3] P. Hrnjak, A.D. Litch, Microchannel heat exchangers for charge minimization in air-cooled ammonia condensers and chillers, Int. J. Refrig. 31 (4) (2008) 658–668.
[4] P. Kumar K, M. Alruqi, H.A. Hanafi, P. Sharma, V.V. Wanatasanappan, Effect of particle size on second law of thermodynamics analysis of Al2O3 nanofluid: application of XGBoost and gradient boosting regression for prognostic analysis, Int. J. Therm. Sci. 197 (2024) 108825.
[5] P.K. Kanti, K.V. Sharma, A.A. Minea, V. Kesti, Experimental and computational determination of heat transfer, entropy generation and pressure drop under turbulent flow in a tube with fly ash-Cu hybrid nanofluid, Int. J. Therm. Sci. 167 (2021) 107016.
[6] P. Kanti, K.V. Sharma, Z. Said, V. Kesti, Entropy generation and friction factor analysis of fly ash nanofluids flowing in a horizontal tube: experimental and numerical study, Int. J. Therm. Sci. 166 (2021) 106972.
[7] M. H B, P.K. Kanti, S.B. Prakash, S.N. Sridhara, Investigation of entropy generation and thermohydraulic characteristics of Al2O3–CuO hybrid nanofluid flow in a pipe at different inlet fluid temperatures, Int. J. Therm. Sci. 193 (2023) 108541.
[8] M. Everts, J.P. Meyer, Relationship between pressure drop and heat transfer of developing and fully developed flow in smooth horizontal circular tubes in the laminar, transitional, quasi-turbulent and turbulent flow regimes, Int. J. Heat Mass Tran. 117 (2018) 1231–1250.

[9] M. Everts, J.P. Meyer, Flow regime maps for smooth horizontal tubes at a constant heat flux, Int. J. Heat Mass Tran. 117 (2018) 1274–1290.
[10] M. Everts, M. Mahdavi, M. Sharifpur, J.P. Meyer, Simultaneous development of the hydrodynamic and thermal boundary layers of mixed convective laminar flow through a horizontal tube with a constant heat flux, Int. J. Therm. Sci. 187 (2023).
[11] A.M. Grishin, V.B. Nemirovskii, Investigation of the flow and heat transfer of viscous reacting fluids in long tubes, Fluid Dynam. 15 (1) (1980) 12–18.
[12] A.J. Ghajar, L.M. Tam, Heat transfer measurements and correlations in the transition region for a circular tube with three different inlet configurations, Exp. Therm. Fluid Sci. 8 (1) (1994) 79–90.
[13] J.P. Meyer, M. Everts, N. Coetzee, K. Grote, M. Steyn, Heat transfer coefficients of laminar, transitional, quasi-turbulent and turbulent flow in circular tubes, Int. Commun. Heat Mass Tran. 105 (2019) 84–106.
[14] J.P. Abraham, E.M. Sparrow, J.C.K. Tong, Heat transfer in all pipe flow regimes: laminar, transitional/intermittent, and turbulent, Int. J. Heat Mass Tran. 52 (3–4) (2009) 557–563.
[15] T.W. Jackson, J.M. Spurlock, K.R. Purdy, Combined free and forced convection in a constant temperature horizontal tube, AIChE J. 7 (1) (1961) 38–41.
[16] D.R. Oliver, The effect of natural convection on viscous-flow heat transfer in horizontal tubes, Chem. Eng. Sci. 17 (5) (1962) 335–350.
[17] A.R. Brown, M.A. Thomas, Combined free and forced convection heat transfer for laminar flow in horizontal tubes, J. Mech. Eng. Sci. 7 (4) (1965) 440–448.
[18] C.A. Depew, S.E. August, Heat transfer due to combined free and forced convection in a horizontal and isothermal tube, J. Heat Tran. 93 (4) (1971) 380–384.
[19] W.W. Yousef, J.D. Tarasuk, Free convection effects on laminar forced convective heat transfer in a horizontal isothermal tube, J. Heat Tran. 104 (1) (1982) 145–152.
[20] D. Bertsche, P. Knipper, T. Wetzel, Experimental investigation on heat transfer in laminar, transitional and turbulent circular pipe flow, Int. J. Heat Mass Tran. 95 (2016) 1008–1018.
[21] M. Everts, M. Mahdavi, J.P. Meyer, M. Sharifpur, Development of the hydrodynamic and thermal boundary layers of forced convective laminar flow through a horizontal tube with a constant heat flux, Int. J. Therm. Sci. 186 (2023).
[22] M. Everts, J.P. Meyer, Laminar hydrodynamic and thermal entrance lengths for simultaneously hydrodynamically and thermally developing forced and mixed convective flows in horizontal tubes, Exp. Therm. Fluid Sci. 118 (2020) 110153.
[23] D. Taler, A new heat transfer correlation for transition and turbulent fluid flow in tubes, Int. J. Therm. Sci. 108 (2016) 108–122.
[24] C.A. Hieber, Laminar mixed convection in an isothermal horizontal tube: correlation of heat transfer data, Int. J. Heat Mass Tran. 25 (11) (1982) 1737–1746.
[25] J.P. Coutier, R. Greif, An investigation of laminar mixed convection inside a horizontal tube with isothermal wall conditions, Int. J. Heat Mass Tran. 28 (7) (1985) 1293–1305.
[26] B. Shome, M.K. Jensen, Mixed convection laminar flow and heat transfer of liquids in isothermal horizontal circular ducts, Int. J. Heat Mass Tran. 38 (11) (1995) 1945–1956.
[27] D. Bertsche, P. Knipper, T. Wetzel, Experimental investigation on heat transfer in laminar, transitional and turbulent circular pipe flow, Int. J. Heat Mass Tran. 95 (2016) 1008–1018.
[28] M. Everts, J.P. Meyer, Heat transfer of developing and fully developed flow in smooth horizontal tubes in the transitional flow regime, Int. J. Heat Mass Tran. 117 (2018) 1331–1351.
[29] S.W. Churchill, H. Ozoe, Correlations for laminar forced convection in flow over an isothermal flat plate and in developing and fully developed flow in an isothermal tube, J. Heat Tran. 95 (3) (1973) 416–419.
[30] B. Shome, M.K. Jensen, Correlations for simultaneously developing laminar flow and heat transfer in a circular tube, Int. J. Heat Mass Tran. 36 (10) (1993) 2710–2713.
[31] Y.S. Muzychka, M.M. Yovanovich, Laminar forced convection heat transfer in the combined entry region of non-circular ducts, J. Heat Tran. 126 (1) (2004) 54–61.
[32] V. Gnielinski, G1 Heat Transfer in Pipe Flow, Springer Berlin Heidelberg, 2010, pp. 691–700.
[33] T.D. Bennett, Correlations for convection in hydrodynamically developing laminar duct flow, J. Heat Tran. 141 (11) (2019) 111701.
[34] B. Jacimovic, S. Genic, D. Lelea, Calculation of the heat transfer coefficient for laminar flow in pipes in practical engineering applications, Heat Tran. Eng. 39 (20) (2018) 1790–1796.
[35] M.A. Akhavan-Behabadi, M.F. Pakdaman, M. Ghazvini, Experimental investigation on the convective heat transfer of nanofluid flow inside vertical helically coiled tubes under uniform wall temperature condition, Int. Commun. Heat Mass Tran. 39 (4) (2012) 556–564.
[36] S.V. Patil, P.V. Vijay Babu, Experimental studies on mixed convection heat transfer in laminar flow through a plain square duct, Heat Mass Tran. 48 (12) (2012) 2013–2021.
[37] D. Bertsche, P. Knipper, K. Kapfer, T. Wetzel, Experimental investigation on heat transfer in laminar, transitional and turbulent circular pipe flow with respect to flow regime boundaries, Int. J. Heat Mass Tran. 145 (2019) 118746.
[38] T.D. Bennett, Laminar convection in circular tubes with developing flow, J. Heat Tran. 142 (11) (2020).
[39] M. Everts, J.P. Meyer, in: J.P. Meyer, M.D. Paepe (Eds.), Test Sections for Heat Transfer and Pressure Drop Measurements: Construction, Calibration, and Validation, The Art of Measuring in the Thermal Sciences, CRC Press, Boca Raton, 2021, pp. 107–158.
[40] C.O. Popiel, J. Wojtkowiak, Simple formulas for thermophysical properties of liquid water for heat transfer calculations (from 0°C to 150°C), Heat Tran. Eng. 19 (3) (1998) 87–101.
[41] P.F. Dunn, Measurement and Data Analysis for Engineering and Science, second ed., CRC Press/Taylor & Francis, Boca Raton, FL, 2010.
[42] R.J. Moffat, Describing the uncertainties in experimental results, Exp. Therm. Fluid Sci. 1 (1) (1988) 3–17.
[43] G.P. Celata, Single and two phase flow transfer in MICROPIPES, in: European Thermal-Sciences Conference, 2008. The Netherlands.
[44] G.l. Maranzana, I. Perry, D. Maillet, Mini- and micro-channels: influence of axial conduction in the walls, Int. J. Heat Mass Tran., 47(17) 3993-4004.
[45] B. Metais, E.R.G. Eckert, Forced, mixed, and free convection regimes, J. Heat Tran. 86 (2) (1964) 295–296.
[46] M. Everts, S. Bhattacharyya, A.I. Bashir, J.P. Meyer, Heat transfer characteristics of assisting and opposing laminar flow through a vertical circular tube at low Reynolds numbers, Appl. Therm. Eng. 179 (2020) 115696.